ELSEVIER

Computational Materials Science 18 (2000) 255–268

COMPUTATIONAL MATERIALS SCIENCE

www.elsevier.com/locate/commatsci

Computing dynamics of copper-based SMA via centre manifold reduction of 3D models ☆

R.V.N. Melnik [a,*], A.J. Roberts [b], K.A. Thomas [b]

[a] *CSIRO Mathematical and Information Sciences – Sydney, Macquarie University Campus, Locked Bag 17, North Ryde, NSW 1670, Australia*

[b] *Department of Mathematics and Computing, University of Southern Queensland, QLD 4350, Australia*

Received 22 November 1999; accepted 6 March 2000

Abstract

In this work, we present a reduction procedure for 3D models describing phase transformations in copper-based shape memory alloys (SMAs) and develop a robust numerical algorithm for the computational analysis of thin single-crystal slabs of these alloys. Starting from a general Landau-type 3D model for the SMA dynamics we have developed a new mathematical "slow manifold" model that allows us to describe effectively the main features of the thermomechanical behaviour of CuAlNi alloys. Results of the mathematical modelling of the thermomechanical fields in CuAlNi SMAs are discussed with numerical examples.

PACS: 65.70+y; 64.70.Kb; 81.30.Kf

Keywords: Copper-based shape memory alloys; Landau-devonshire phenomenology; Centre manifold technique

1. Introduction

Shape-memory alloys (SMAs) are an intrinsic part of smart material and structure (SMS) technology with a wide variety of applications in such areas as aerospace engineering, medicine, manufacturing (including automotive industry and consumer products), civil infrastructure systems, biomechanics, oceanographic research, vibration control and suppression.

A smart structure is a non-biological physical structure having a definite purpose, means and imperatives to achieve that purpose and a biological pattern of functioning [1]. Smart materials are assumed to be a subset of smart structures considered at the microscopic or mesoscopic scales. Materials such as an optical fibre or a surface acoustic wave device (having the sensing function), piezoelectronic devices or SMAs (having the actuating function) are in this category. Closely related to SMS technology is the concept of intelligent materials. These materials are often defined as materials which respond to environmental

☆ This paper is based on the authors' contribution to the European Conference on Computational Mechanics, Munich, 1999.

* Corresponding author. Tel.: +61-2-9325-3247; fax: +61-2-9325-3200.
E-mail address: roderick.melnik@cmis.csiro.au (R.V.N. Melnik).

0927-0256/00/$ - see front matter
PII: S0927-0256(00)00104-X

changes, adjust themselves toward the optimum conditions, and manifest their functions according to these changes [2]. In addition to sensor and actuator functions, an intelligent material has to have "build-in" processor and feedback functions. Key areas of industrial research in the SMS technology are centred around (a) piezoelectric materials, (b) shape-memory materials, (c) magnetostrictive materials, (d) electro- and magneto-rheological fluids, (e) optical fibres and feedback control systems.

In this paper, we address the adequate mathematical description of the dynamic behaviour of SMAs, materials with a rapidly expanding market of commercial exploitations [3]. SMAs are sensitive to both temperature and applied stress, and their thermomechanical properties are effectively used in the production of medical/biomedical devices (such as superelastic orthodontic archwires and optic lens holders), in minimally invasive surgery, control devices for robotics, sensor/actuator functional elements and many other applications in SMS technology [4].

The mathematical modelling of shape-memory materials and the analysis of associated models have become areas of increasing interest in the engineering, computational mechanics, and applied mathematics communities [4–13]. This interest has two major sources: on the one hand, a wide range of important industrial applications of shape-memory materials; and on the other hand, a class of very challenging mathematical problems that arise in modelling the dynamics of these materials.

This paper is organised as follows:

- In Section 2, we describe main properties of SMAs that are of industrial importance with the emphasis on copper-based alloys and explain the major difficulties in computational studies of these materials.
- In Section 3, we provide the analysis of different scales used in the modelling of SMA dynamics.
- Section 4, provides the reader with a 3D Landau-type model used as a core model in our analysis.
- In Section 5, we apply a computer algebra implementation of slow manifold analysis to give a systematic approach for the modelling of thermomechanical behaviour of SMAs on the mesoscopic scale.
- Some computational results obtained with our new model are presented in Section 6.
- Conclusion and future directions are discussed in Section 7.

2. Thermomechanical properties of copper-based SMAs

Under the action of thermal, mechanical, magnetic, hydrostatic or other fields some materials may restore their original shapes after being deformed. This property is usually termed the shape-memory effect and has been observed in a number of material systems such as metals, ceramics and polymers.

Although a large variety of materials can exhibit the shape memory effect, only those that

- can recover a substantial amount of strain or
- generate significant force upon changing shape

are of current industrial interest. The key in the wide applicability of SMAs is in a displacive diffusionless process, called the first-order martensitic phase transformation, which leads to an internal structural change in the material where in certain temperature regimes two different phases (austenite and martensite) may coexist. We aim for the adequate description of the dynamics of this transformation using tools of mathematical modelling and computational experiment. At present, amongst the SMA family nickel–titanium (NiTi) and copper-based alloys are the most important. Mechanical properties of these materials vary greatly over the temperature range spanning their transformation. This brings difficulties in determining thermomechanical characteristics of SMAs. For example, if the temperature is slightly above the transformation temperature for this material, we observe a non-linear pseudoelasticity effect. In this case, the material becomes extremely elastic and the elastic characteristics of the material (such as Young's modulus) become strongly dependent on both temperature and strain deformation. Below we give a brief overview of thermomechanical characteristics of copper-based alloys, in particular copper–aluminium–nickel.

Despite its wide commercial exploitation, NiTi in finished form is very expensive, and in many applications Cu-based alloys such as CuZnAl and CuAlNi provide a more economical alternative to NiTi [14]. Compared to NiTi, a lower recoverable strain of the copper-based SMAs (around 4% compared to 8.5% for NiTi) has been making these alloys very attractive for the design of different types of actuators.

Perhaps one of the most important advantage of copper-based alloys lies with the fact that they have transformation temperatures well above NiTi alloys. Therefore, where higher temperature actuation is required, CuAlNi alloys are usually preferred since they can give a recovery temperature of up to 190–200°C (the melting temperature is 1000–1050°C) [15]. According to Hodgson, Wu and Biermann (see `http://www.sma-inc.com`), with the density 7.12 g/cm^3 commercially available CuAlNi alloys have a thermal conductivity coefficient within 30–43 W/(m °C) and a heat capacity 373–574 J/(kg °C). These alloys have the yield strength around 400 MPa in the β parent phase and 130 MPa in the martensite (Young's modulus is 85 GPa in the β parent phase and 80 GPa in the martensite), whereas their ultimate tensile strength is up to 500–800 MPa.

Thermomechanical characteristics of CuAlNi have made these SMAs the most appropriate for switching elements in circuit breakers and many other applications [16]. Copper-based SMAs are becoming more and more important in consumer goods manufacturing and are now used in fire protection devices, in actuators for anti-scald safety valves etc. However, note that these materials are quite sensitive to brittleness (at low temperatures) and instability (they are metastable in nature). The resistivity of these alloys is only 11–13 μΩ cm compared to 100 μΩ cm in the austenite state (70 μΩ cm in the martensite state) for nickel–titanium alloys. This leads to considerable difficulties in modelling the dynamics of CuAlNi alloys undergoing thermally and mechanically induced thermoelastic martensitic transformations. Due to its intrinsic metastability, in practical applications this material often requires training (i.e., a progressive modification of the admissible mixtures of martensites and austenite, produced by thermomechanical treatments of the alloy) in order to retain the parent β-phase for shape-memory effects.

Our main results in this paper concern copper-based SMAs, in particular copper–aluminium–nickel alloys.

3. Hierarchy of models for cubic-to-monoclinic phase transformations in copper-based SMAs

The first step in the construction of mathematical and computational models for the analysis of thermomechanical behaviour of SMAs is the choice of an appropriate spatial length scale. In principle, such models can be constructed on any of the atomic-, meso- or macro-scale levels. However, the deformation process of the phase transformation simulated on the computer will be strongly dependent on the length of observation. In the majority of current applications, the required length of observation may vary from a few nanometers to hundreds of micrometers ($\approx 10^{-9}$–10^{-4} m).

Using the Landau–Devonshire phenomenology, established by Falk on the mesoscopic scale, in our earlier papers (see [9] and references therein) we performed a computational analysis of the austenitic–martensitic phase transitions of SMAs described by the following model:

$$
\begin{aligned}
&C_v\left[\frac{\partial\theta}{\partial t}+\tau_0\frac{\partial^2\theta}{\partial t^2}\right]-k_1\left[\theta\frac{\partial u}{\partial x}\frac{\partial^2 u}{\partial t\,\partial x}+\tau_0\frac{\partial}{\partial t}\left(\theta\frac{\partial u}{\partial x}\frac{\partial^2 u}{\partial t\,\partial x}\right)\right]-\mu\left[\left(\frac{\partial^2 u}{\partial t\,\partial x}\right)^2+\tau_0\frac{\partial}{\partial t}\left(\frac{\partial^2 u}{\partial t\,\partial x}\right)^2\right]\\
&\quad-\nu\left[\frac{\partial\theta}{\partial t}\frac{\partial^2 u}{\partial t\,\partial x}+\tau_0\frac{\partial}{\partial t}\left(\frac{\partial\theta}{\partial t}\frac{\partial^2 u}{\partial t\,\partial x}\right)\right]-\frac{\partial}{\partial x}\left(k\frac{\partial\theta}{\partial x}\right)=G,\\
&\rho\frac{\partial^2 u}{\partial t^2}-\frac{\partial}{\partial x}\left[k_1\frac{\partial u}{\partial x}(\theta-\theta_1)-k_2\left(\frac{\partial u}{\partial x}\right)^3+k_3\left(\frac{\partial u}{\partial x}\right)^5\right]-\mu\frac{\partial^3 u}{\partial x^2\,\partial t}-\nu\frac{\partial^2\theta}{\partial x\,\partial t}=F,
\end{aligned}
\tag{3.1}
$$

where u is the displacement field, θ the temperature field, τ_0 the thermal relaxation time, k the thermal conductivity of the material, C_v the specific heat constant of the material, μ and ν material-specific coefficients that characterise the dependency of the stress on the rate of the deformation gradient and temperature, respectively, ρ the density of the material, θ_1 a positive constant that characterises a critical temperature of the material, and k_i, $i = 1, 2, 3$, are material-specific constants that characterise the material's free energy. The right-hand sides of system (3.1), F and G, represent distributed mechanical and thermal loadings of the body.

Although this model was developed on the mesoscale level, it should be noted that the connection between different levels of descriptions manifests itself in the constitutive theories where one has to couple (a) the free energy, (b) the stress, and (c) the heat flow of the crystal with deformation, temperature and, when necessary, with their temporal and spatial gradients (see [9] and references therein). When only equilibrium properties of the material are of interest, such theories can be simplified with the stress represented by the derivative of the free energy function with respect to deformation. In model (3.1), we used the phenomenological Landau–Devonshire free energy function and the Cattaneo–Vernotte model for heat conduction. The shear strain on the habit plane (the contact plane between both phases) was taken as the basic deformation variable. In some cases we have to deal with habit planes of discontinuous deformation (for example, considering domain walls between martensitic variants, nucleation phenomena, or studying the interface between martensite and austenite). One way of dealing with such situations is to incorporate the Ginzburg term into the model (modify the Landau–Devonshire free energy function by adding the couple stresses term). Apart from the fact that this approach is disputable [17], it appeared that with reported values of the Ginzburg coefficient (10^{-10}–10^{-12}) the gradient strain term has a negligible effect in the class of experiments we performed (see [9] and references therein). As we shall see in Section 5 a similar situation arises when the 3D Landau-type model is reduced to 1D.

The model (3.1) was completed by appropriate initial and boundary conditions and was solved with respect to (u, θ) in the spatial–temporal region $Q = \{(x, t) \mid 0 \leqslant x \leqslant L,\ 0 \leqslant t \leqslant T_f\}$, where L is the length of the structure and T_f is the required time of observation. The initial conditions for the model (3.1) were taken in the following form:

$$u(x,0) = u^0(x), \quad v(x,0) = \frac{\partial u}{\partial t}(x,0) = u^1(x), \quad \theta(x,0) = \theta^0(x), \quad \frac{\partial \theta}{\partial t}(x,0) = \theta^1(x), \tag{3.2}$$

with specified functions u^0, u^1, θ^0, θ^1. Boundary conditions are problem-specific (see [9] and references therein). In our experiments, mechanical boundary conditions were either specified stress or specified displacement,

$$s(0,t) = s_1(t), \quad s(L,t) = s_2(t) \quad \text{or} \quad u(0,t) = u_1(t), \quad u(L,t) = u_2(t); \tag{3.3}$$

thermal boundary conditions are those of specified heat flux

$$\frac{\partial \theta}{\partial x}(0,t) = \bar{\theta}_1(t), \quad \frac{\partial \theta}{\partial x}(L,t) = \bar{\theta}_2(t), \tag{3.4}$$

where functions $s_i(t)$ (or $u_i(t)$) and $\bar{\theta}_i(t)$, $i = 1, 2$ were given.

In this paper, we continue investigation of mesoscale models of the Landau-type with the emphasis on the modelling of the copper-based SMA copper–aluminium–nickel. Recall that in the parent high temperature phase (austenite) the copper-based SMAs (such as CuZnAl and CuAlNi) have an ordered body-centred cubic (bcc) lattice. In the phase transformation "each" cubic cell of austenite is transformed into a tetragon, forcing the parent phase to be transformed to an ordered and twinned martensite. Therefore, it is fundamental to this type of transformations that both the parent austenitic phase and the martensitic product are ordered. In the general case, one has to deal with 24 crystallographically equivalent martensitic

variants (due to the transformation from the 48th order cubic symmetry group of the parent phase to the 2nd order monoclinic group of the product phase). The twinning property of the martensite is the result of minimisation of the stress on the habit plane. Therefore, as follows from the Falk deformation theory [10], due to high interface mobilities between martensite variants and between austenite and martensite variants, for the shape memory effect to occur this plane should be invariant. However, on the *micro-deformation level* (where only the lattice deformation, i.e., the Bain strain, is taken into account) the invariant habit plane does not exist [10]. Indeed, in the martensitic phase transformation the atomic displacements are very small and one can assume that no atomic migration is required for this transformation. Atoms cooperatively rearrange to form a new crystal structure. As a result of this assumption on the *mesoscale deformation level* we consider a coupled effect of the Bain strain and the lattice-invariant shearing mechanism. In the copper-based alloys of interest (CuZnAl and CuAlNi) the lattice-invariant strain is realised as a regular twinning on layers resulting from $\{1\ 1\ 0\}$-planes (called twinning or basal planes) of the bcc lattice (every third layer twins to form a large monoclinic martensite unit cell). It is this coupling effect between the Bain strain and the regular twinning that leads to "almost" invariant plane strain, i.e., a stress-free interface between austenite and martensite.

Now, when the habit plane is stress-free the sheared martensitic volume element will not fit into the region it occupied when it was in the austenitic state [10]. However, this problem is easily solved on the *macroscopic deformation level* where we assume that the martensitic inclusion does not form as a single martensitic variant. A self-accommodating group of martensitic variants is formed into an aggregate of several martensitic variants, the so-called domain (sometimes called a microstructure) [10,18]. For such domains the average deformation of their components cancel out. Due to this, on cooling the phase transformation from austenite to martensite occurs without a macroscopic shape change (scale of 10^{-4} m or larger) exhibiting a "ferroelastic" type of stress–strain curves. However, when the transformation is induced by a stress, in the temperature range where the stress-free austenite is stable, we have to deal with pseudoelastic stress–strain curves. One of the approaches that allow work on the macroscopic scale (where the deformation defined on a length scale of 100 μm or more) stems from Frémond's work (see references in [11]) and is based on the introduction of an internal variable that characterises fractions of austenite and martensite variants in SMAs. We shall not consider this approach in this paper. We only note that one may expect that the Landau theory on the mesoscale level used in this paper is a consequence of the Landau theory on the microscale level and the constitutive relations of the macroscopic theories (including the Frémond theory) have to follow from the Landau theory considered on the mesoscale level. However, the construction of the hierarchy

$$\text{Microscale Landau theory} \Rightarrow \text{Mesoscale Landau theory} \Rightarrow \text{Macroscopic theories}$$

is just at the beginning of its development [10]. Hereafter, we concentrate on a particular Landau-type models developed on the mesoscale level [19].

4. 3D Landau-type phenomenological models for the dynamics of SMAs

Numerical analysis of Landau-type models for the description of SMA dynamics has been typically restricted to the 1D case [5,12,13]. 3D modelling in this field is traditionally associated with the application of Frémond's type models [11]. At the time of writing this paper, we are not aware of any computational results obtained with the later models for physically realistic data. The Frémond models consider the phase proportions as thermodynamic quantities and typically include strain gradient terms to account for interfacial energies. This leads to a smoothing term in the momentum balance equation and simplifies analytical analysis of the models (see also Section 3). In the terminology discussed in Section 3, Frémond's models are considered on the macroscopic scale with temperature, macroscopic strain, strain gradient and

the volumetric proportions of austenite and martensites (usually restricted by only two variants) being state variables. Such macroscale models ignore the internal atomic and mesoscale structures of a material using the assumption that the phases simultaneously present *at each point* of the material with appropriate proportions. In this case, we have to deal with self-accommodating groups of martensite as a result of the deformation of a macroscopic sample, as explained in the previous section. We are concerned with a smaller scale, which, however, is larger than the scale of the monoclinic lattice (i.e., the Bain strain is beyond the resolution of our models). More precisely, our models describe the phase-transition between bcc austenite and monoclinic martensite variants on the mesoscopic scale. In order to describe the macroscopic behaviour of SMAs an additional averaging (over the different martensite variants forming the macroscopic sample) procedure is required (see [19] and references therein).

Mathematical description of the appropriate mesoscale measure starts from the approximation by a polynomial (with coefficients depending on temperature) with respect to an order parameter characterising the phase transformation as follows (see e.g., [9,19] and references therein):

$$\Psi(\boldsymbol{\epsilon},\theta)=\psi^0(\theta)+\sum_{i=1}^{\infty}\psi^i(\boldsymbol{\epsilon},\theta), \tag{4.1}$$

where independent material parameters of the nth order for $n=1,2,\ldots$ are determined through strain invariants, $\mathscr{I}_j^n$ as follows:

$$\psi^n=\sum_{j=1}^{j^n}\psi_j^n\mathscr{I}_j^n \quad \text{and} \quad \psi^0(\theta)=\psi_0^0(\theta). \tag{4.2}$$

To make the free energy function invariant with respect to the symmetry group of austenite, the upper limit of the sum in (4.2), j^n, is chosen as the number of all invariant directions associated with a representation of the 48th order cubic symmetry group of the parent (austenite) phase.

For the copper-based alloys it is possible to reduce the number of required parameters in (4.1) to only 10 material constants (in the general case, temperature-dependent) [19]

$$\Psi=\psi^0(\theta)+\sum_{i=1}^{3}\psi_i^2\mathscr{I}_i^2+\sum_{i=1}^{5}\psi_i^4\mathscr{I}_i^4+\sum_{i=1}^{2}\psi_i^6\mathscr{I}_i^6, \tag{4.3}$$

where the strain invariants $\mathscr{I}_i^n$ of second, fourth and sixth orders of the 48th order cubic symmetry group of the parent phase are determined as follows:

$$\begin{aligned}
&\mathscr{I}_1^2=\frac{1}{9}(\mathrm{tr}(\epsilon_{ij}))^2, \quad \mathscr{I}_2^2=\frac{1}{12}(2\epsilon_{33}-\epsilon_{11}-\epsilon_{22})^2+\frac{1}{4}(\epsilon_{11}-\epsilon_{22})^2,\\
&\mathscr{I}_3^2=\epsilon_{23}^2+\epsilon_{13}^2+\epsilon_{12}^2, \quad \mathscr{I}_1^4=(\mathscr{I}_2^2)^2, \quad \mathscr{I}_2^4=\epsilon_{23}^4+\epsilon_{13}^4+\epsilon_{12}^4, \quad \mathscr{I}_1^6=(\mathscr{I}_2^2)^3,\\
&\mathscr{I}_3^4=(\mathscr{I}_3^2)^2, \quad \mathscr{I}_4^4=\mathscr{I}_2^2\mathscr{I}_3^2,\\
&\mathscr{I}_5^4=\epsilon_{23}^2\left[\frac{1}{6}(2\epsilon_{33}-\epsilon_{11}-\epsilon_{22})-\frac{1}{2}(\epsilon_{11}-\epsilon_{22})\right]^2+\epsilon_{13}^2\left[\frac{1}{6}(2\epsilon_{33}-\epsilon_{11}-\epsilon_{22})+\frac{1}{2}(\epsilon_{11}-\epsilon_{22})\right]^2\\
&\qquad+\frac{1}{9}\epsilon_{12}^2(2\epsilon_{33}-\epsilon_{11}-\epsilon_{22})^2, \mathscr{I}_2^6=\frac{1}{36}(2\epsilon_{33}-\epsilon_{11}-\epsilon_{22})^2\left(\frac{1}{36}(2\epsilon_{33}-\epsilon_{11}-\epsilon_{22})^2-\frac{1}{4}(\epsilon_{11}-\epsilon_{22})^2\right)^2.
\end{aligned} \tag{4.4}$$

Due to the symmetry, the strain tensor ϵ_{ij}, $i,j=1,2,3$ forms a 6D space with the basis $\phi_K, K=1,\ldots,6$ [20]

$$\boldsymbol{\epsilon}=\sum_{K=1}^{6}\epsilon_K\phi_K, \tag{4.5}$$

where

$$\epsilon_1 = \epsilon_{11}, \quad \epsilon_2 = \epsilon_{22}, \quad \epsilon_3 = \epsilon_{33}, \quad \epsilon_4 = 2\epsilon_{23}, \quad \epsilon_5 = 2\epsilon_{13}, \quad \epsilon_6 = 2\epsilon_{12}. \tag{4.6}$$

We assume that the strain tensor is coupled to the spatial displacements $\mathbf{u} = (u_1, u_2, u_3)$ of the material point with Lagrangian coordinates $\mathbf{x} = (x_1, x_2, x_3)$ at time t by the Cauchy relation

$$\epsilon_{ij}(\mathbf{x}, t) = \frac{1}{2}\left[\frac{\partial u_i(\mathbf{x}, t)}{\partial x_j} + \frac{\partial u_j(\mathbf{x}, t)}{\partial x_i}\right], \quad i, j = 1, 2, 3. \tag{4.7}$$

Finally, to complete the definition of the free energy function (4.3) we specify the parameters ψ_i^j ($j = 0,\ i = 0$; $j = 2,\ i = 1, 2, 3$; $j = 4,\ i = 1, \ldots, 5$; $j = 6,\ i = 1, 2$) which for the copper–aluminium–nickel alloys (Cu is 14 wt% and Al is 3 wt%) are

$$\begin{aligned}
&\psi_1^2 = 5.92 \times 10^6 \mathrm{g/(ms^2\ cm)}, \quad \psi_2^2 = (1.41 \times 10^5 + 46(\theta - 300))\mathrm{g/(ms^2\ cm)},\\
&\psi_3^2 = (1.48 \times 10^6 + 940(\theta - 300))\mathrm{g/(ms^2\ cm)}, \quad \psi^0 = -\alpha_1\theta \ln[(\theta - \theta_0)/\theta_0]\mathrm{g/(ms^2\ cm)},\\
&\psi_1^4 = (-1.182 \times 10^8 + 3.55 \times 10^5(\theta - 300))\mathrm{g/(ms^2\ cm)},\\
&\psi_2^4 = 3.13 \times 10^9 \mathrm{g/(ms^2\ cm)}, \quad \psi_3^4 = 1.64 \times 10^9 \mathrm{g/(ms^2\ cm)},\\
&\psi_4^4 = -5.53 \times 10^8 \mathrm{g/(ms^2\ cm)}, \quad \psi_5^4 = -4.27 \times 10^8 \mathrm{g/(ms^2\ cm)},\\
&\psi_1^6 = 3.35 \times 10^{10} \mathrm{g/(ms^2\ cm)}, \quad \psi_2^6 = 3.71 \times 10^{11} \mathrm{g/(ms^2\ cm)},
\end{aligned} \tag{4.8}$$

where α_1 is the heat capacity of the material.

Having the free energy function, we define the shear stress by its three components: The quasi-conservative component, $\mathbf{s}^{\mathrm{q}}$, the stress component due to mechanical dissipation, $\mathbf{s}^{\mathrm{m}}$, and the stress component due to thermal dissipations, $\mathbf{s}^{\mathrm{t}}$, (the latter is assumed to be negligible),

$$\mathbf{s} = \mathbf{s}^{\mathrm{q}} + \mathbf{s}^{\mathrm{m}} + \mathbf{s}^{t} \quad \text{with } \mathbf{s}^{\mathrm{q}} = \rho\frac{\partial \Psi}{\partial \boldsymbol{\epsilon}},\ \mathbf{s}^{\mathrm{m}} = \rho\mu\frac{\partial \boldsymbol{\epsilon}}{\partial t},\ \mathbf{s}^{\mathrm{t}} = \mathbf{0}. \tag{4.9}$$

If we assume that $\mu = 0$, then the relationship $\mathbf{s} = \mathbf{0}$ (i.e., the derivative of the free energy function with respect to $\boldsymbol{\epsilon}$) gives the necessary conditions for the minima of Ψ. Although we have six such conditions (see the representation (4.5)), we are only interested in the conditions associated with austenite and martensite phases. The first such condition, $\boldsymbol{\epsilon} = \mathbf{0}$, is associated with the austenite phase which is stable when the Hessian of Ψ (computed with respect to $\boldsymbol{\epsilon}$) is positive definite. The second condition, derived in [19],

$$\boldsymbol{\epsilon} = \begin{pmatrix} 2\alpha & \beta & 0 \\ \beta & 0 & -\beta \\ 0 & -\beta & -2\alpha \end{pmatrix} \tag{4.10}$$

corresponds to a monoclinic spontaneous strain with temperature-dependent parameters α and β subject to the following system of equations [19]:

$$\begin{aligned}
&48\alpha^4\psi_1^6 + 8\alpha^2\psi_1^4 + 2\beta(\psi_4^4 + \psi_5^4) + \psi_2^2 = 0,\\
&4\alpha^2(\psi_4^4 + \psi_5^4) + 2\beta^2(\psi_2^4 + 2\psi_3^4) + \psi_3^2 = 0.
\end{aligned} \tag{4.11}$$

Given α^2, from (4.11) we deduce β^2 and then the magnitude of the shear strain vector by the formula [19]

$$|\boldsymbol{\epsilon}|^2 = 2\left[1 - \sqrt{1 - 8(2\alpha^2 + \beta^2)}\right]. \tag{4.12}$$

The strain invariants in this situation are

$$\begin{aligned}
&\mathscr{I}_1^2 = 0, \quad \mathscr{I}_2^2 = 4\alpha^2, \quad \mathscr{I}_3^2 = 2\beta^2, \quad \mathscr{I}_1^4 = 16\alpha^4, \quad \mathscr{I}_2^4 = 2\beta^4,\\
&\mathscr{I}_3^4 = 4\beta^4, \quad \mathscr{I}_4^4 = 8\alpha^2\beta^2, \quad \mathscr{I}_5^4 = 8\alpha^2\beta^2, \quad \mathscr{I}_1^6 = 64\alpha^6, \quad \mathscr{I}_2^6 = 0.
\end{aligned} \tag{4.13}$$

For the given temperature, these relations allow us to define the stress and the free energy function as functions of the monoclinic spontaneous strain defined by the matrix (4.10).

Now, we are in the position to describe the dynamics of SMAs in the 3D case by the coupled system that consists of the equation of motion and the energy balance equation

$$\begin{aligned} &\rho\frac{\partial^2\mathbf{u}}{\partial t^2} = \nabla_{\mathbf{x}}\cdot\mathbf{s} + \mathbf{F},\\ &\rho\frac{\partial e}{\partial t} - \mathbf{s}^T : (\nabla\mathbf{v}) + \nabla\cdot\mathbf{q} = g, \end{aligned} \tag{4.14}$$

where $\mathbf{F}$ and g are given distributed mechanical and thermal loadings of the body and $\mathbf{a}^T : \mathbf{b} = \sum_{i,j=1}^{3} a_{ij}b_{ij}$ is the standard notation for the rank 2 tensors $\mathbf{a}$ and $\mathbf{b}$. The velocity function $\mathbf{v}$, the internal energy function, e and the heat flux, $\mathbf{q}$ are defined as follows:

$$\mathbf{v} = \frac{\partial\mathbf{u}}{\partial t}, \quad e = \Psi - \theta\frac{\partial\Psi}{\partial\theta}, \quad \mathbf{q} = -k\nabla\theta - \alpha\frac{\partial k\nabla\theta}{\partial t}, \tag{4.15}$$

where the last expression is an approximation to the solution of the 3D Cattaneo–Vernotte equation [9] (computational experiments were performed with the classical Fourier law where $\alpha = 0$).

The embedding of constitutive equations that couples the free energy, the stress and the heat flow with the state variables into the basic laws of mechanics (4.14) provides the foundation for the mathematical modelling of SMA dynamics. Of course, the specification of constitutive equations for shape memory materials is far from being unique and the development of thermodynamic constitutive models for these materials is an active area of research [6–8,21]. Recently, Lurier [6] proposed a quite general approach to the construction of constitutive models for SMAs (a number of earlier developed structural–analytical, phenomenological and micromechanical models follow from his model as special cases). Although we do not consider these constitutive models here, in Section 5 we develop a computer algebra-based technique which, with appropriate modifications, is capable of effectively incorporating those models.

5. Low-dimensional slow manifold models for the dynamics of SMAs

We consider an SMA slab which is very large in the $x = x_1$ direction compared to its thickness of $2b$ in the $y = x_2$ direction ($-b < y < b$) and neglect any motion and dependence in the x_3 direction. In this section, we reduce the 3D model for the dynamics of SMAs described in Section 4 to a simpler model expressed in terms of the amplitudes of cross-sectional averages of critical quantities. The basic idea of our approach is to express the physical fields in terms of asymptotic sums in these amplitudes and their longitudinal gradients. The asymptotic approximation is found to solve the system (4.14) describing the dynamics of SMA. This technique is at the heart of centre manifold theory, originated by Pliss [22]. During the last decade this technique has been successfully linked to computer algebra approaches and applied to a number of problems in continuum mechanics (e.g., [23,24]). It is this linkage that makes the centre manifold method a powerful tool in the analysis of complex mathematical models. We refer the reader to [25,26] (and the references therein) for the rigorous analysis of the reduction procedure of a system onto a centre manifold. Here, using similar techniques, we develop the slow, sub-centre manifold [27, Section 7] model by adapting the analysis of beam theory developed by [28] to the non-linear dynamics of SMA. We show, using the computer algebra package REDUCE, how to derive systematically (up to the arbitrary order of accuracy) an accurate low-dimensional model for the description of thermomechanical behaviour of thin slabs in SMA materials.

For the unforced dynamics ($\mathbf{F} = \mathbf{0}, g = 0$) we derive a model that describes the dynamics of slowly varying (along the slab) modes. We note that in the presence of a time-dependent forcing, the system may

substantially deviate from the slow manifold and the use of geometric projection of initial conditions is required to determine the forcing appropriate for the model. As for the boundary conditions, the theory typically employs arguments based on the spatial evolution away from the boundary which are applied to the original model and its approximation (see [24] and references therein). Here, we use "zero-stress" and "thermal-insulation" boundary conditions specified on $y = \pm b$, and "pinned" and "insulating ends" boundary conditions provide a leading approximation in the "long" direction (this, however, requires a quite delicate analysis which is outside the scope of this paper [24]).

We model the long-wavelength, small-wavenumber modes along the slab. For simplicity in this first approach, we also assume that the effect of dissipation processes is negligible (we set $\alpha = \mu = 0$). Then, the eigenvalue analysis of the cross-slab modes shows that generally there is a zero eigenvalue of multiplicity five which corresponds to large-scale longitudinal waves, large-scale bending, and one heat mode (since dissipation effects were neglected, all other eigenvalues are pure imaginary). Thus, there exists a slow sub-centre manifold based on these five modes. This fact allows us to construct a new model on the sub-centre manifold (although the model will not have an assured guarantee of asymptotic completeness [23,25,26]).

Since the leading order structure of the critical eigenmodes is constant across the slab, the amplitudes of the critical modes are chosen to be the cross-sectional averages

$$U_i(x,t) = \overline{u_i}, \quad V_i(x,t) = \overline{v_i}, \quad \Theta'(x,t) = \overline{\theta'}, \tag{5.1}$$

where an overbar denotes the y-average quantity and $\theta' = \theta - \theta_0$ ($\theta_0 = 300$ K). Our low-dimensional model is written in terms of these parameters. We seek the low-dimensional invariant manifold upon which these amplitudes evolve slowly

$$u_i = \mathscr{U}_i(\boldsymbol{U}, \boldsymbol{V}, \Theta'), \quad v_i = \mathscr{V}_i(\boldsymbol{U}, \boldsymbol{V}, \Theta'), \quad i = 1,2, \quad \theta = \mathscr{T}(\boldsymbol{U}, \boldsymbol{V}, \Theta'), \tag{5.2}$$

where

$$\frac{\partial U_1}{\partial t} = V_i, \quad \frac{\partial V_1}{\partial t} = g_i(\boldsymbol{U}, \boldsymbol{V}, \Theta'), \quad \frac{\partial \Theta'}{\partial t} = g_\theta(\boldsymbol{U}, \boldsymbol{V}, \Theta'). \tag{5.3}$$

The expression (5.2) is substituted into the model (4.14) and the resulting system is solved to some order in the small parameters ∂_x, $E = \|\boldsymbol{U}_x\| + \|\boldsymbol{V}_x\|$ and $\vartheta = \|\Theta'\|$ with the computer algebra package REDUCE. Thus, here we treat the strains as small, as measured by E, while permitting asymptotically large displacements and velocities.

We use $\mathscr{O}(E^p + \partial_x^q + \vartheta^r)$ to denote an error in the model obtained by neglecting all terms involving $\partial_x^{\beta_1} E^{\beta_2} \vartheta^{\beta_3}$ such that $\beta_1/p + \beta_2/q + \beta_3/r \geqslant 1$. Then, with errors $\mathscr{O}(E^5 + \partial_x^{5/2} + \vartheta^{5/2})$ the displacement and temperature fields of the slow manifold, in terms of the amplitudes and the scaled transverse coordinate $Y = y/b$, are

$$u_1 \approx U_1 - YbU_{2x} + 0.15(3Y^2 - 1)b^2 U_{1xx}, \tag{5.4}$$

$$u_2 \approx U_2 - (0.9 - 3.05\mathrm{e}-5\Theta')YbU_{1x} + 0.15(3Y^2 - 1)b^2 U_{2xx} - 141YbU_{1x}^3 + 1.00\mathrm{e}-4(3Y - Y^3)b^3 V_{1x}^2 U_{1x}, \tag{5.5}$$

$$\theta \approx 300 + \Theta' - 2.43\mathrm{e}6(3Y - Y^3)b^3(V_{1x}U_{2xx} + U_{1x}V_{2xx}) - 25.1(7 - 30Y^2 + 15Y^4)V_{1x}^3 U_{1x}. \tag{5.6}$$

The mechanical and thermal field approximations represented by (5.4)–(5.6) have cross-slab structure (e.g., [9]). In particular, the sideways deformation u_2 (which is a non-linear function of the longitudinal strains) of the SMA feedback at higher order to contribute to and complicate the longitudinal and thermal dynamics. The computer algebra code to derive these expressions is available upon request to the authors. Finally, with errors $\mathscr{O}(E^8 + \partial_x^4 + \vartheta^4)$ the model for the longitudinal dynamics on this slow manifold is

$$
\begin{aligned}
\rho\frac{\partial V_1}{\partial t} &= c_1 U_{1xx} + \gamma_1 b^2 U_{1xxxx} \\
&\quad + \partial_x\Big[(c_2\Theta' - c_3\Theta'^2)U_{1x} - (c_4 - c_5\Theta')U_{1x}^3 + c_6 U_{1x}^5 \\
&\quad + (c_7 - c_8\,\Theta')b^2 V_{1x}^2 U_{1x} + c_9\, b^4 V_{1x}^4 U_{1x} - c_{10} b^2 V_{1x}^2 U_{1x}^3\Big], \\
\rho\frac{\partial V_2}{\partial t} &= -\gamma_2 b^2 U_{2xxxx}, \\
C_v\frac{\partial \Theta'}{\partial t} &= \kappa\Theta'_{xx} + (c_{11} + c_{12}\,\Theta' - c_{13}\,\Theta'^2)U_{1x}V_{1x} \\
&\quad + (c_{14} + c_{15}\,\Theta')V_{1x}U_{1x}^3 + c_{18}V_{1x}U_{1x}^5 \\
&\quad - (c_{16} + c_{17}\,\Theta')b^2 V_{1x}^3 U_{1x} - c_{19} b^2 V_{1x}^3 U_{1x}^3 - c_{20}\, b^4 V_{1x}^5 U_{1x} \\
&\quad + c_{21} b^2 U_{1xx}V_{1xx} + c_{22} b^2 U_{2xx}V_{2xx} + \partial_x^2[-c_{23}\, b^2 U_{1x}V_{1x}], \\
\frac{\partial U_i}{\partial t} &= V_i, \quad i = 1, 2,
\end{aligned}
\tag{5.7}
$$

where coefficients c_k, $k = 1, \ldots, 23$, are positive material constants.

In the first equation of this system the first line in the right-hand side describes linear dispersive elastic waves along the slab, whereas the second line gives the temperature-dependent quintic stress–strain relation of the SMA (the analogue of the classical Falk representation). The remaining terms describe the effects due to rates of change of the strain (see [9] and references therein). The first two lines in the right-hand side of the third equation of the system describe the diffusion of heat generated/absorbed by mechanical strains, $\Theta U_{1x}^p V_{1x}$ terms. The remaining lines show the effects of the internal pattern of mesoscopic strain. Finally, note that since there is no coupling of the longitudinal dynamics to the bending modes of the slab (to this order of truncation), the second equation of the system is the classic beam equation.

6. Computational implementation and numerical examples

Computational experiments reported in this section were performed for a thin single-crystal CuAlNi slab. The thermomechanical parameters for this material were chosen to be (see Section 2)

$$
\rho = 7.12\ \text{g/cm}^3, \quad k = 0.0030\ \text{cm g/(ms}^3\ \text{K)}, \quad C_v = \rho\alpha_1 = 26.6\ \text{g/(ms}^2\ \text{cm K)}. \tag{6.1}
$$

By assuming the slab is thin enough so that in effect $b = 0$ we reduce our model (5.7) to the following differential–algebraic system:

$$
\begin{aligned}
\rho\frac{\partial V_1}{\partial t} &= \frac{\partial s}{\partial x} + F, \\
C_v\frac{\partial \Theta'}{\partial t} &= k\frac{\partial^2\Theta'}{\partial x^2} + (c_{11} + c_{12}\Theta' - c_{13}(\Theta')^2)\frac{\partial U_1}{\partial x}\frac{\partial V_1}{\partial x} + (c_{14} + c_{15}\theta')\frac{\partial V_1}{\partial x}\left(\frac{\partial U_1}{\partial x}\right)^3 \\
&\quad + c_{18}\frac{\partial V_1}{\partial x}\left(\frac{\partial U_1}{\partial x}\right)^5 + g, \\
s &= (c_1 + c_2\theta' - c_3(\theta')^2)\frac{\partial U_1}{\partial x} - (c_4 - c_5\theta')\left(\frac{\partial U_1}{\partial x}\right)^3 + c_6\left(\frac{\partial U_1}{\partial x}\right)^5, \\
\frac{\partial U_1}{\partial t} &= V_1.
\end{aligned}
\tag{6.2}
$$

This system is then discretised in space using second-order approximations in space on staggered grids and solved with the differential–algebraic solver described in our earlier papers (e.g., [9] and references therein).

The coefficients in the model (6.2) are obtained directly from the model (5.7) and CuAlNi alloys have the following numerical values:

$$\begin{aligned} &c_1 = 1.91 \times 10^6, \quad c_2 = 592, \quad c_3 = 0.00931, \quad c_4 = 2.75 \times 10^9, \quad c_5 = 8.42 \times 10^6, \\ &c_6 = 4.56 \times 10^{11}, \quad c_{11} = 1.78 \times 10^5, \quad c_{12} = 586, \quad c_{13} = 5.94, \quad c_{14} = 2.53 \times 10^9, \\ &c_{15} = 8.11 \times 10^6, \quad c_{18} = 1.08 \times 10^{12}, \quad \gamma_1 = 5.15 \times 10^5. \end{aligned} \tag{6.3}$$

If the thickness of the slab is not negligible compared to its length (taken to be 1 cm in our experiments), then the inclusion of all b-dependent terms in the model (6.2) is required. The corresponding coefficients for CuAlNi have the following values:

$$\begin{aligned} &c_7 = 1811, \quad c_8 = 5.64, \quad c_9 = 0.728, \quad c_{10} = 2.51 \times 10^3, \quad c_{16} = 36.8, \quad c_{17} = 0.00761, \\ &c_{18} = 1.08 \times 10^{12}, \quad c_{19} = 1.016 \times 10^6, \quad c_{20} = 0.0116, \quad c_{21} = 1.05 \times 10^4, \\ &c_{22} = 5.92 \times 10^4, \quad c_{23} = 5228, \quad \gamma_2 = 6.36 \times 10^5. \end{aligned} \tag{6.4}$$

In the first experiment we study the dynamics of a shape memory alloy sample under the uniform mechanical forcing $F = -1 \times 10^{-3}$ g/(μs^2 cm^2) and time-dependent distributed heating/cooling according to the rule $g = 1.15 \times 10^{-3}\pi \sin^3(t\pi/15)$ g/(μs^3 cm). The initial displacement field was taken to be

$$u^0(x) = \begin{cases} 0.0636x, & 0 \leqslant x \leqslant 1/2, \\ 0.0636(1-x), & 1/2 \leqslant x \leqslant 1. \end{cases} \tag{6.5}$$

We used "pinned ends" and "thermal insulation" boundary conditions. With the initial temperature 350 K, the dynamics of the sample on the time interval $0 \leqslant t \leqslant 30$ μs are presented in Fig. 1. On heating, the

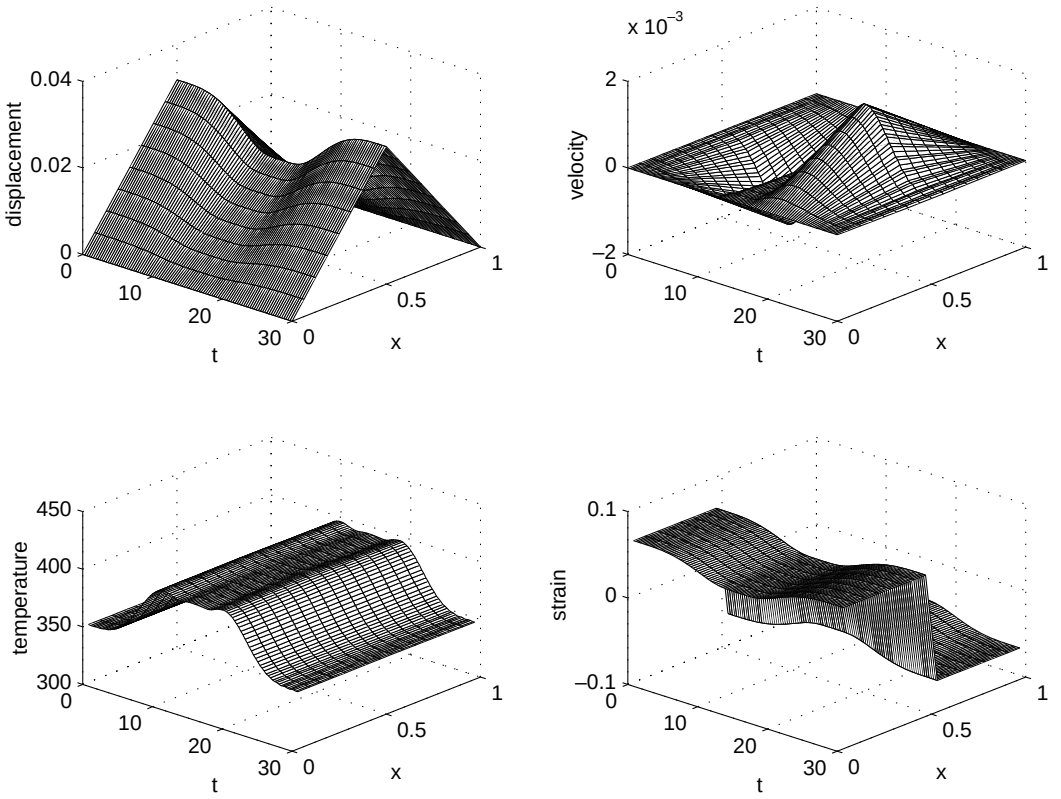

Fig. 1. Thermal forcing of a CuAlNi slab.

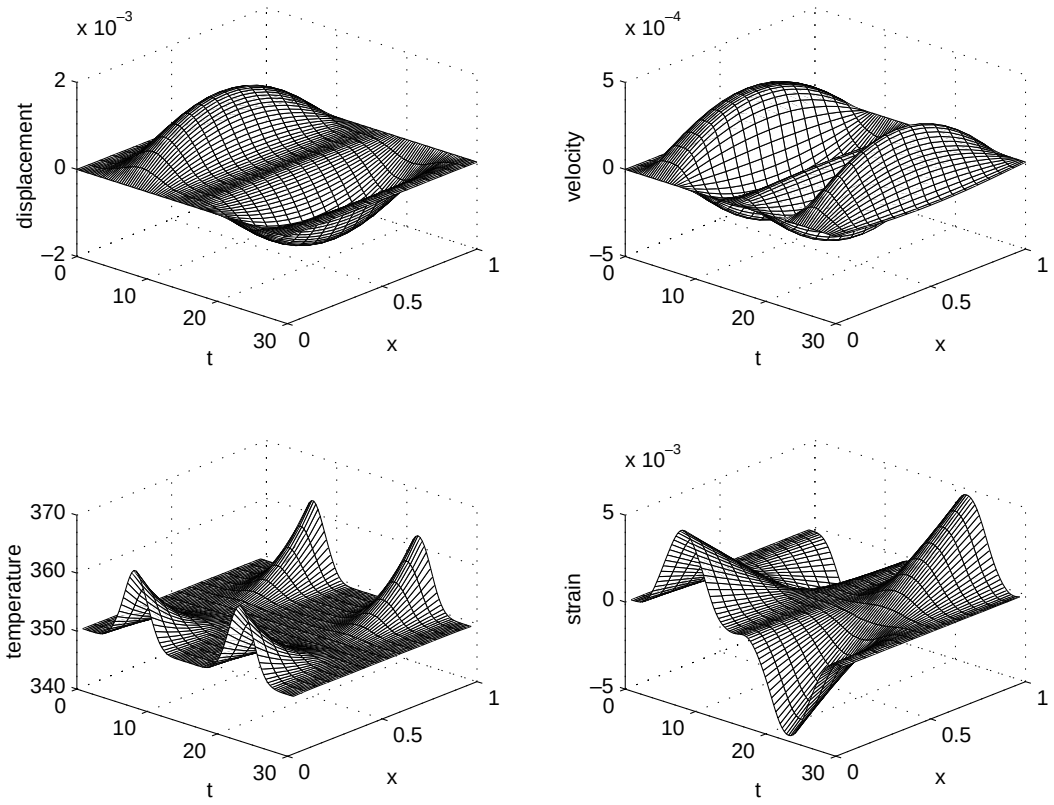

Fig. 2. Mechanical forcing of a CuAlNi slab.

martensite phase becomes metastable. Under appropriate thermomechanical conditions, this metastability may lead to the transformation of martensite phase into austenite. An attempt of this transformation is accompanied by a certain decrease in temperature, clearly visible in Fig. 1. This decrease compensates for the given thermal forcing and the resulting temperature is insufficient to transform martensite into austenite on this scale of observation. Therefore, on cooling, the martensite phase returns to its original stable state.

The second experiment uses a purely mechanical ($g = 0$) time-dependent forcing given by the formula $F = 0.03\sin^3(\pi t/15)$ g/(cm^2 μs^2). We use the same boundary conditions as before. Starting with the initial configuration $u^0 = 0$ at the temperature 350 K we observe a strong coupling phenomenon between thermal and mechanical fields (see Fig. 2). This phenomenon reminds us of our earlier results (see [9] and references therein), where the dynamics of AuCuZn alloys were investigated. It is evident that it is much more difficult to retain the austenite phase in copper–aluminium–nickel compared to AuCuZn alloys and the computational analysis of stability of the parent phase for CuAlNi requires further investigation.

7. Conclusions

In this paper, we presented results of an investigation into the thermomechanical behaviour of a copper–aluminium–nickel SMA. Using the 3D Landau theory describing the martensitic phase transformation of SMAs, we developed a systematic approach to the SMA modelling based on centre manifold techniques

implemented in computer algebra packages. In particular, we constructed a new model for the description of the SMA dynamics that allows us to describe essential dynamic behaviour of the system by determining the evolution on the crucial subset of all possible modes. The numerical scheme based on an effective differential–algebraic integrator provides a robust approach to the analysis of SMA dynamics. This analysis has been used in computational studies of thermomechanical behaviour of CuAlNi alloys.

The implementations of computational results into engineering applications are impeded by the absence of a theory that would allow us to compute thermomechanical characteristics of polycrystallines using such characteristics for single-crystal. Effective averaging procedures over the grains are required in order to transfer highly non-linear stress–strain curves for single-crystals to polycrystals [10,18]. Using such procedures, the technique proposed in our paper can be effectively adapted to the analysis of SMA dynamics in polycrystalline structures as well as to other problems on structural phase transitions.

Acknowledgements

This research was supported by the Australian Research Council Grant 179406.

References

[1] W.B. Spillman, J.S. Sirkis, P.T. Gardiner, Smart materials and structures: what are they?, Smart Mater. Struct. 5 (1996) 247–254.
[2] T. Takagi, Recent research on intelligent materials, J. Intell. Mater. Systems Struct. 7 (1996) 346–352.
[3] N.B. Morgan, C.M. Friend, Market strategies for the commercial exploitation of shape memory alloys, J. Phys. IV France (Colloque C5) 7 (1997) 615–620.
[4] J. Van Humbeeck, Shape memory materials: state of the art and requirements for future applications, J. Phys. IV France (Colloque C5) 7 (1997) 3–12.
[5] M. Niezgodka, J. Sprekels, Convergent numerical approximations of the thermomechanical phase transitions in shape memory alloys, Numer. Math. 58 (1991) 759–778.
[6] S.A. Lurier, On thermodynamical constitutive relations for shape memory materials, Mech. Solids 5 (1997) 110–122.
[7] J.G. Boyd, D.C. Lagudas, A thermodynamic constitutive model for shape memory materials Part 1, Int. J. Plasticity 12 (6) (1996) 805.
[8] V.G. DeGiorgi, H. Saleem, A comparison of a few shape memory alloy constitutive models, In: V.V. Varadan (Ed.), Mathematics and Control in Smart Structures, Proceedings of SPIE, vol. 3667, 1999, pp. 730–737.
[9] R.V.N. Melnik, A.J. Roberts, K.A. Thomas, Modelling dynamics of shape-memory-alloys via computer algebra, In: V.V. Varadan (Ed.), Mathematics and Control in Smart Structures, Proceedings of SPIE, vol. 3667, 1999, pp. 290–301.
[10] F. Falk, On constitutive theories of shape memory alloys undergoing a structural phase transformation, Mater. Sci. Forum 123–125 (1993) 91–100.
[11] P. Colli, J. Sprekels, Global existence for a three-dimensional model for the thermo-mechanical evolution of shape memory alloys, Nonlinear Analysis: TMA 18 (1992) 873–888.
[12] K.-H. Hoffmann, J. Zou, Finite element approximations of Landau–Ginsburg's equation model for structural phase transitions in shape memory alloys, M^2AN 29 (1995) 629–655.
[13] O. Klein, Stability and uniqueness results for a numerical approximation of the thermomechanical phase transitions in SMA, Adv. Math. Sci. Appl. (Tokyo) 5 (1) (1995) 91–116.
[14] M.H. Wu, Cu-based shape memory alloys, in: T.W. Duering (Ed.), Engineering Aspects of Shape Memory Alloys, Butterworths, London, 1990, pp. 69–88.
[15] L. McDonald Schetky, Shape memory alloy applications in space systems, in: T.W. Duering (Ed.), Engineering Aspects of Shape Memory Alloys, Butterworths, London, 1990, pp. 170–177.
[16] E. Runtsch, Shape memory actuators in circuit breakers, in: T.W. Duering (Ed.), Engineering Aspects of Shape Memory Alloys, Butterworths, London, 1990, pp. 330–337.
[17] J. Sprekels, Shape memory alloys: mathematical models for a class of first order solid–solid phase transitions in metals, Control Cybernet. 19 (3/4) (1990) 287–308.
[18] M. Luskin, On the computation of crystalline microstructure, Acta Numer. 5 (1996) 191–257.
[19] F. Falk, P. Konopka, Three-dimensional Landau theory describing the martensitic phase transformation of shape-memory-alloys, J. Phys.: Condens. Matter 2 (1990) 61–77.

[20] P. Konopka, F. Falk, Three-dimensional Landau theory describing the martensitic phase transformation of shape-memory alloys, Mater. Sci. Forum 123–125 (1993) 113–122.
[21] E.J. Graesser, F.A. Cozzarelli, A proposed three-dimensional constitutive model for shape memory alloys, J. Intell. Mater. Systems Struct. 5 (1994) 78–89.
[22] V.A. Pliss, A reduction principle in the theory of stability of motion, Izv. Akad. Nauk. SSSR. Ser. Mat. 28 (1964) 1297–1324.
[23] S.M. Cox, A.J. Roberts, Centre manifolds of forced dynamical systems, J. Austral. Math. Soc. Ser. B 32 (1991) 401–436.
[24] A.J. Roberts, Low-dimensional modelling of dynamics via computer algebra, Comput. Phys. Commun. 100 (1997) 215–230.
[25] L.P. Shilnikov et al., Center Manifold. Local Case, In: L.P. Shilnikov et al. (Eds.), Methods of Qualitative Theory in Nonlinear Dynamics. Part 1, World Scientific, Singapore, 1990, pp. 269–323.
[26] Th. Gallay, A center-stable manifold theorem for differential equations in Banach spaces, Commun. Math. Phys. 152 (1993) 249–268.
[27] J. Sijbrand, Properties of centre manifolds, Trans. Am. Math. Soc. 289 (1985) 431–469.
[28] A.J. Roberts, The invariant manifold of beam deformations part 1:the simple circular rod, J. Elas. 30 (1993) 1–54.